WPMAT-PR(18) 20713

A Platonenko et al.

First principles simulations on migration paths of oxygen interstitials in magnesium aluminate spinel

Preprint of Paper to be submitted for publication in
Physica Status Solidi

This work has been carried out within the framework of the EUROfusion Consortium and has received funding from the Euratom research and training programme 2014-2018 under grant agreement No 633053. The views and opinions expressed herein do not necessarily reflect those of the European Commission.

WILEY-VCH

DOI: 10.1002/ ((please add manuscript number))
Article type: Full Paper

First principles simulations on migration paths of oxygen interstitials in magnesium aluminate spinel

*Alexander Platonenko, Denis Gryaznov, Yuri F. Zhukovskii, Eugene A. Kotomin**

Alexander Platonenko, Dr. Denis Gryaznov, Dr. Yuri F. Zhukovskii, Dr. Eugene A. Kotomin
Institute of Solid State Physics, University of Latvia, 8 Kengaraga, Riga LV-1063, Latvia
E-mail: E.Kotomin@fkf.mpg.de

Keywords: radiation defects, magnesium-aluminium spinel, interstitial oxygen, diffusion, first principles calculations

Thermal stability of the primary electronic defects – *F* type centers – in oxide materials is controlled by their recombination with much more mobile complementary defects – interstitial oxygen ions O_i. Thus, the study of interstitial ion migration is of key importance for the prediction of radiation damage in oxides. In this study, several possible migration trajectories for neutral and charged interstitial oxygen ions were calculated in $MgAl_2O_4$ spinel using the first principles calculations of atomic and electronic structure. The lowest energy barriers are ~1.0–1.1 eV and 0.8 eV, respectively. The effective atomic charges, charge redistribution, and lengths of bonds closest to O_i interstitials are analysed in detail.

1. Introduction

Several radiation-resistant binary and ternary oxides (MgO, Al_2O_3, $MgAl_2O_4$) are considered as perspective candidates for the diagnostics/optical windows in fusion devices.[1-3] As is known, accumulation of radiation-induced defects affects optical and other properties of optical components. Thus, understanding of the defect stability and recombination becomes very important issue. It was suggested [4, 5] that $MgAl_2O_4$ crystalline structure exhibits a very high tolerance to irradiation with fast neutrons due to efficient recombination of primary Frenkel defects – vacancies and interstitials (i-v pairs). The decisive factor for such self-healing recombination process is a huge concentration of structural or native vacancies in the

cation sublattice of a normal spinel [3]: cations occupy only one-eighth of the available tetrahedral sites (Mg^{2+}) and one-half of the available octahedral sites (Al^{3+}). Therefore, there exists additional efficient mechanism for the accommodation of Frenkel defects induced via elastic collisions of neutrons in the $MgAl_2O_4$ lattice, such as exchanging the positions of cations between tetrahedral and octahedral sites resulting in the so-called *antisite defects*. The primary defects in the oxygen sublattice are known as the *F* type centers (oxygen vacancies with trapped electrons) and complementary interstitial oxygen ions, O_i. The former defects reveal characteristic optical absorption and are well identified whereas the latter are studied quite poorly. It is well known also that in most ionic solids, including alkali halides [6, 7] and binary oxides [8, 9], anion interstitials are much more mobile than the *F* centers and thus control their recombination rate and defect concentrations. There were several experimental [3, 5, 10] and theoretical first principles [11] studies of radiation defects in $MgAl_2O_4$ mostly focused on the electronic centers, whereas O_i interstitials are studied very poorly. So far, only a few theoretical studies have been performed for O_i in MgO [12] and α-Al_2O_3 [9] predicting split interstitial (dumbbell) configuration as energetically the most preferable. Analogous conclusions were drawn also for neutral O_i interstitials in perfect $MgAl_2O_4$ bulk based on both first principles [13] and classical pair-potential [14] calculations. One of open questions is, in which charge state O_i migrates in magnesium-aluminium spinel and how the charge state affects its migration energy. As we demonstrated for sapphire [15], migration energy for a charged interstitial oxygen could be considerably smaller than for the neutral one. Thus, the main aim of this study is first principles calculations of the interstitial oxygen migration in $MgAl_2O_4$ bulk for different charge states.

2. Computational details and defect model

Magnesium aluminate spinel $MgAl_2O_4$ crystal containing radiation point defects – interstitial oxygen atoms and F-centers (O_i or F) were simulated using linear combination of atomic orbitals method within density functional theory (LCAO-DFT) approach. To perform spin polarized calculations, we employed the linear combination of atomic orbitals and a screened hybrid HSE06 exchange-correlation functional with the fraction of exact exchange of 25% and screening length of 0.2 A^{-1} as implemented in CRYSTAL17 computer code. [16,17] We used the all-electron basis sets (BS) of atomic Gaussian type functions (GTFs) both for O atoms (6*s*-2111*sp*-1*d*) [18], as well for Mg atoms (8*s*-511*sp*-1*d*).[19] Alternatively, for Al atoms, the effective core pseudopotential (ECP) proposed by Durand, with 21*sp*-1*d* external shell has been used.[20]

To minimize the interaction between O_i defects in a periodic spinel model, supercells of two sizes were used: a conventional cell of 56 atoms (four primitive unit cells) and 2×2×2 supercell (eight primitive unit cells) of 112 atoms. The reciprocal space integration has been performed by sampling the Brillouin zone with the 6×6×6 Monkhorst-Pack mesh [21] for 56 atom supercell and 4×4×4 for 112 atom supercell. Calculations of point defects were performed using standard geometry optimization and energy minimization procedure.[16] Convergence criteria was set to 10^{-7} a.u. for self-consistency procedure. The effective charges on atoms were evaluated using two different methods: Mulliken population analysis [22] and Hirshfeld-I method [23] as implemented into the CRYSTAL17 code, whereas the bond properties were made using TOPOND code.[24] Direct frozen phonon method was used for vibrational frequency calculations.[25, 26] The formation energies for point defects were calculated using the equations:

$$E_{form}^{O_i} = E_{total}^{O_i} - E_{total}^{Mg\,Al_2O_4(perfect)} - 1/2\,E_{total}^{O_2}, \quad (1)$$

$$E_{form}^{V_O} = E_{total}^{V_O} - E_{total}^{Mg\,Al_2O_4(perfect)} + 1/2\,E_{total}^{O_2}, \quad (2)$$

where $E_{total}^{O_i ¿ V_O}$ is the total electronic energy of the spinel supercell containing defect, $E_{total}^{Mg\,Al_2O_4(perfect)}$ - the total electronic energy of a perfect supercell, and $E_{total}^{O_2}$ - the total electronic energy of oxygen molecule.

To estimate migration barriers for Oi in spinel, we used a similar approach as was described by us in [15]. The ground-state configuration (dumbbell in case of neutral O*i*) of defect was chosen as the starting point for migration for both neutral and charged O_i. Geometry optimization of migration paths were performed in redundant internal coordinates. One coordinate, the distance between O_i and regular oxygen atom O_{reg}, was frozen on each step whereas all other internal coordinates including angles were optimized fully. For each migration path, 8-12 configurations were calculated depending on path length. We assume that oxygen vacancy is well-separated from oxygen interstitial, so it does not affect oxygen atom migration. To calculate charged O_i, uniform background charge density neutralized the negative charge in the reference cell. [16]

For the crystallographic parameters of $MgAl_2O_4$ we obtained the lattice constant a = 8.064 Å and internal coordinate u = 0.264 which are in good agreement with experimental values a = 8.081 Å and u = 0.2623, respectively. [27] The calculated bandgap at the Γ-point is 8.70 eV which only slightly overestimates the experimental value of 7.8 eV. [28] The effective charges calculated by Mulliken analysis (q_{Mg}^{eff}=¿ +1.63*e*, q_{Al}^{eff}=¿ +1.44*e*, q_{O}^{eff}=¿ -1.13*e* are lower than those obtained by Hirsfeld-I method (q_{Mg}^{eff}=¿ +2.0*e*, q_{Al}^{eff}=¿ +2.48*e*, q_{O}^{eff}=¿ -1.74*e*. Both methods clearly show that Mg-O bond is fully ionic (zero bond population), while Al-O bond nature is mixed ionic-covalent. As it was shown for corundum [23], Mulliken population analysis demonstrated an O-Al electron back-donation which is also observed in spinel.

3. Results and discussion

3.1 Formation energies and basic properties for oxygen interstitial defects

In our previous study the site-symmetry approach was applied to describe neutral oxygen interstitials defects in $MgAl_2O_4$.[13] It was found that high symmetry configurations provided higher formation energies, while asymmetrical configuration is more preferable. According to results obtained for 56 and 112 atom supercells (**Table 1**), the ground-state configuration for oxygen interstitial in a spinel is the O_i–O_{reg} pair (known also as the *dumbbell* or *split interstitial*) centered at a regular oxygen lattice site. We found similar dumbbell configurations in previous calculations for O_i in MgO [12] and sapphire.[29] However, unlike binary oxides, the regular O_{reg} site is occupied here asymmetrically: one of dumbbell O atoms forms two Al-O bonds, while a second O forms only one Al-O bond and has a stronger ionic interaction with Mg atom. The initially neutral O_i atom attracts additional electronic density, which results in almost symmetrical charge distribution between the two oxygen atoms in the dumbbell. For better understanding of the dumbbell O_i–O_{reg} properties, we performed vibrational frequency and density of states calculations, as well as used topological analysis of the electron density, according to Quantum Theory of Atoms in Molecules (QTAIM). [30, 31]

The defect formation energies are found to be close for both size supercells. Removing oxygen atom and creating a vacancy V_O resulted in formation of additional occupied level in the band gap. About two electrons were localized on outer orbitals of three nearest aluminium atoms. The absorption energy of this defect is 5.7 eV **(Figure 1)**, which is close to experimentally observed absorption band (~5.3 eV) for *F*-centers in spinel.[3]

The analysis of the electronic density for neutral oxygen interstitial defect reveals a covalent bonding between two oxygen atoms. Total effective charge of O_i–O_{reg} dumbbell is lower than the effective charge of oxygen atom in perfect spinel, because some charge density is redistributed toward Al atom to form a new bond. The dumbbell contains no unpaired electrons and its ground state is singlet. Plotted 2D Laplacian $\nabla^2\rho$ (Figure 4) of electron

density makes the atomic shell structure visible, which cannot be observed through the topology of ρ. Large negative values of $\nabla^2\rho$ oriented towards two atoms (high density blue lines in Figure 4) confirm the formation of O_2 (consisting of O_i and O_{reg}) in the dumbbell configuration. The interatomic distance in the dumbbell of 1.42 Å lies in-between 1.33 Å, typical for superoxides $O2^-$, and 1.49 Å, typical for peroxide $O2^{2-}$ [32] and close to our finding for the dumbbell in sapphire (see also ref. [29] and table 3 therein). The total effective charge of O_i–O_{reg} pair found by two methods (Mulliken: -1.26*e*, Hirschfeld-I:-1.67*e*) is smaller than could be expected for peroxide species (-2*e*). Lastly, the calculated O_i-O_{reg} vibrational frequency of 1142 cm^{-1} in spinel is characteristic for superoxide $O2^-$ ion (1145 cm^{-1} [32]). The possible explanation for reduced charge can be that the part of O *2p* electron density are involved in the Al-O bond formation, and remaining electrons form O_i–O_{reg} bond, what results in formation of occupied bonding σ orbital and empty antibonding σ^* orbital, while the 2*p*-orbitals, one on each of the two atoms, are not hybridized and maintain an atom-like character. This idea also can be confirmed by density of states (**Figure 2**), where two occupied levels lie at the top of the valence band, and unoccupied σ^* orbital is ~8 eV higher in energy. The NEXAFS measurements of O 1s → σ^* excitation in various peroxides report values about 8.3–8.8 eV for that transition. [33]

It is possible within the LCAO formalism to add one electron on p-orbitals of O_i atom (called, hereafter, Oi-). After the full electronic and structure relaxation it results in the significant changes in the O-O pair properties. The interatomic distance results in the significant changes in the O-O pair configuration. The interatomic distance becomes larger by 0.5 Å and increases up to 1.95 Å. The charge and spin density is equally distributed between the two atoms (-1.28*e* and 0.45μ_B by Hirshfeld-I, as well as -0.92 *e* and 0.48μ_B by Mulliken), resulting in the formation of pseudo-dumbbell, even though calculations of vibrational frequencies do not reveal common stretching O-O vibrational mode. The interpretation of

DOS (Figure 2) in this case becomes more complicated. Additional electron could occupy only σ^* orbital (in the O_2 molecular orbitals diagram), and that would result in breaking the O–O bond. Performing the electron density analysis, we found that weak interaction is still present between the two oxygen atoms. Oxygen anions in such pseudo-dumbbells are kept together not by chemical bonding but more likely through interaction with surrounding cations. Thus, the occupation of σ^* orbital can be more energetically favourable than other configurations without O–O interactions since in other oxides oxygen interstitials occupying octahedral or tetrahedral sites are unstable.

3.2 Migration paths of O_i atom in spinel

The difference in defect energies and charges between two used supercells is very small, so the 56 atom supercell can be considered as a good choice for further modelling single point defects. Still, the larger supercell was used in migration barrier calculations, to avoid possible artefacts.

The migration paths and the calculated energy curves are shown in **Figure 3**. Three regular oxygen atoms nearest to O_i (within 2.5 A distance) were selected as a final position for migration, leaving its partner in dumbbell (O_{reg0} in **Figure 4**, dotted box in Figure 3) and moving to another regular oxygen ion ($O_{reg\text{-}2/3}$ in Figure 4). Migration paths can be described as one-dimensional diffusion: path I lies along <100> direction, paths II and III are oriented along <110> direction. While path II passes unoccupied tetrahedral 8*b* interstice, path III lies near Mg atom occupying 8*a* site (both sites are defined in Ref. [13]). All paths reveal a clear energy barrier and end up with the formation of a new O-O pair with the regular oxygen atom. Estimated barriers lie in the range from 1 eV to 2.4 eV (**Table 2**). For more detailed analysis, we take a closer look on surroundings of O_i and the electron density distribution in starting/final point (considered as equivalent) and the top of barrier.

The two paths, I and II, with low energy barrier have practically identical saddle points. Moving along the paths O_i attracts electron density from O_{reg2}, while O_{reg0} gets its normal charge as in perfect crystal. It is also reflected in the positive values of $\nabla^2\rho$ (red colour contours between O_i and O_{reg0} in Figure 4). At the saddle point O_i attracts 0.5*e* in total, almost equally from both oxygen atoms. A closer look at the saddle point of path III clearly shows that the rise in energy barrier occurs due to a strong interaction with Mg atom. At the same time, the O–O bond lengths and populations are very similar to paths I and II. The only difference is interaction with Mg atom instead of Al atom. This effect could be especially important for Mg-rich spinels, where antisite defects Mg_{Al} are common, which could affect oxygen migration. Actually stoichiometric $MgAl_2O_4$ exhibits some inversion (typically for synthetic materials i=0.1 in $(Mg_{1-i}Al_i)(Mg_iAl_{2-i})O_4$). So the present results are relevant to understanding the difference between normal and partly inverted spinel met often in real situations. Also, in absence of strong Al–O interaction, Mulliken and Hirshfeld-I methods give similar results for O_i effective charge. Migration barriers of ~1 eV are smaller than calculated for neutral oxygen interstitials in corundum (~1.3 eV) and MgO (1.45 eV). If we assume that limiting step for neutral oxygen interstitial migration is O–O bond breaking, it can be concluded that asymmetrical surrounding of the dumbbell in spinel could decrease this bond energy.

3.3 Migration paths of O_i^- ion in spinel

In contrast with a neutral O_i, *charged* oxygen O_i^- ion in spinel forms a pseudo-dumbbell which symmetrically occupies a regular oxygen site: each of two oxygen atoms forms the covalent bonds with 2 Al atoms and one ionic bond with Mg atom. Within 1NN oxygen atoms, there exist two symmetrically inequivalent migration paths for interstitial migration (**Figure 5**). As was mentioned previously, charged oxygen interstitial has a weaker O-O bond,

what also can be seen on the Laplacian of electron density maps by its value being close to zero (grey color in **Figure 6**).

Similar to the migrations paths of neutral O*i* atom, path I is oriented along <100> direction and path II along <110>. Calculated migration paths show smaller energy barriers (~0.8-0.9 eV) than for neutral O*i*. Surrounding of oxygen interstitial in a top of migration barrier (**Table 3**) also differs comparing to neutral one: along path I, O*i* breaks one of two bonds with Al, has weak interaction with O_{reg1}, and makes additional ionic bond with one more Mg ion to compensate negative charge. As a result, path is curved that way, so it goes through middle point between two Mg ions (Figure 6). Along path II, O*i* is not interacting with Mg ions and preserves two Al–O bond along all the path, what could be an explanation for slightly higher energy barrier.

4 Conclusions

We have presented results on large-scale *ab initio* calculations on defective aluminium magnesium spinel containing neutral and single-charged oxygen interstitial defects. For both, neutral and charged, oxygen interstitials interaction with magnesium ions plays an important role in defining migration barrier. Calculated activation energies are ~1 eV for neutral, and 0.8 eV for charged oxygen interstitials. Previously reported data on intertitial mobility in $MgAl_2O_4$ estimates migration barrier ~0.4 eV from the analysis of the denuded zone of dislocation loops at a grain boundary[34], and molecular dynamics simulations suggesting 0.64-0.67 eV for unconstrained 3D diffusion of O_i^{2-} specie. [35] Increase of charge of oxygen interstitial decreases energy barrier for migration. While neutral O_i creates covalent bond with regular oxygen, charged O_i^- has very weak O-O interaction due to σ^* orbital occupation (but for O_i^{2-} orbital overlaping with O_{reg} will be energetically unfavourable due to double occupation of σ^* orbital). Although higher negative charge results in stronger bonding with cations, the mobility of charged O_i^- is higher. This leads us to conclusion, that O_i-O_{reg}

interaction may be considered as the limiting step for oxygen diffusion in spinel. However, to be sure in such conclusion, it is neccesary to study mobility of O_i in presence of hole center (cation vacancy or Mg_{Al} antisite), which would result in even stronger O_i-O_{reg} bonding, than in case of neutral O_i. The difficulties for comprasion of the results with experimental data arise from the fact that the most of direct measurments of point defect mobility was done for irradiated $MgAl_2O_4$ samples, where ionizing radiation produces also numbers of antisite defects and cation vacancies.[3] In this study we have used model of perfect spinel crystal without antisite defects and zero degree of inversion. For the exploring influence of other defects, further calculations of oxygen intertitial near the Mg_{Al} and Al_{Mg} sites will be performed.

Acknowledgments

This work has been carried out within the framework of the EUROfusion Consortium and has received funding from the Euratom research and training programme 2014–2018 under grant agreement No 633053. The authors are indebted to R.A. Evarestov, A.I. Popov, A.C. Lushchik and R. Vila for stimulating discussions. The views and opinions expressed herein do not necessarily reflect those of the European Commission. Calculations have been performed using Marconi supercomputer system based in Italy at CINECA Supercomputing Centre.

References (format pss)

[1] A. Ibarra, E. R. Hodgson, Nucl. Inst. Meth. B **218** (2004) 29

[2] F. Mota, C. J. Ortiz, R. Vila, N. Casal, A. Garcia, A. Ibarra, J. Nucl. Mater. **442** (suppl. 1) (2013) 5699

[3] A. Lushchik, S. Dolgov, E. Feldbach, R. Pareja, A. I. Popov, E. Shablonin, V. Seeman, Nucl. Inst. Meth. B *in press*, (2017) http://dx.doi.org/10.1016/j.nimb.2017.10.018

[4] D. Bacorisen, R. Smith, B. P. Uberuaga, K. E. Sickafus, Phys. Rev. B **74** (2006) 214105

[5] P.B. Uberuaga, M. Tang, C. Jiang, J.A. Valdez, R. Smith, Y. Wang, K. E. Sikafus, Nat. Commun. **6** (2015) 8750

[6] A. Lushchik, Ch. Lushchik, K. Schwartz, E. Vasil'chenko, T. Karner, I. Kudryavtseva, V. Issakhanyan, A. Shugai, Nucl. Inst. Meth. B **266** (2008) 2868

[7] V. N. Kuzovkov, A. I. Popov, E. A. Kotomin, A. M. Moskina, E. Vasil'chenko, A. Lushchik, Low Temp. Phys. **42** (2016) 748

[8] E. A. Kotomin, A. I. Popov, Nucl. Inst. Meth. B **141** (1998) 1

[9] E. A. Kotomin, V. N. Kuzovkov, A. I. Popov, R. Vila, Nucl. Inst. Meth. B **374** (2016) 107

[10] J-M. Costantini, G. Leiong, M. Guillaumet, W. J. Weber, S. Takaki, K. Yasuda, J. Phys. Cond. Matt. **28** (2016) 325901

[11] S. Jiang, T. Lu, Y.I. Long, J. Chen, J. Appl. Phys. **111** (2012) 043516

[12] T. Brudevoll, E.A. Kotomin, N. E. Christensen, Phys. Rev. B **53** (1996) 773

[13] R. A. Evarestov, A. Platonenko, Yu. F. Zhukovskii, Comput. Mater. Sci. **150** (2018) 517

[14] C.A. Gilbert, R. Smith, S.D. Kenny, S.T. Murphy, R.W. Grimes, J.A. Ball, J. Phys. Cond. Matt. **17** (2009) 275406

[15] A. Platonenko, D. Gryaznov, Yu.F. Zhukovskii, E.A. Kotomin, *Nucl. Instrum.Meth. Phys. Res. B* (2018) *in press*, https://doi.org/10.1016/j.nimb.2017.12.022.

[16] R. Dovesi, V. R. Saunders, C. Roetti, R. Orlando, C. M. Zicovich-Wilson, F. Pascale, B. Civalleri, K. Doll, N. M. Harrison, I. J. Bush, P. D'Arco, M. Llunell, M. Causà, Y. Noël, L. Maschio, A. Erba, M. Rerat, S. Casassa, CRYSTAL17 User's Manual (2017). University of Torino, Torino.

[17] A. V. Krukau, O. A. Vydrov, A. F. Izmaylov, G. E. Scuseria, J. Chem. Phys. **125** (2006) 224106

[18] J. Baima, A. Erba, M. Rérat, R. Orlando, R. Dovesi, J. Phys. Chem. C **117** (2013) 12864

[19] M.I. McCarthy, N. M. Harrison, Phys. Rev. B **49** (1994) 8574

[20] P. Durand, J.C. Barthelat. *Theor. Chim. acta* **38** (1975) 283

[21] H. J. Monkhorst, J. D. Pack, Phys. Rev. B. **13** (1976) 5188

[22] R. S. Mulliken, I. J. Chem. Phys. **23** (1955) 1833

[23] C. M. Zicovich-Wilson, M. Hô, A. M. Navarrete-López, S. Casassa, Theor. Chem. Acc. 135 (2016) 188

[24] C. Gatti, Zeitschrift fur Kristallographie **220** (2005) 399

[25] F. Pascale, C. M. Zicovich-Wilson, F. Lopez Gejo, B. Civalleri, R. Orlando, R. Dovesi, J. Comput. Chem. **25** (2004) 888

[26] C. M. Zicovich-Wilson, F. Pascale, C. Roetti, V. R. Saunders, R. Orlando, R. Dovesi, J. Comput. Chem. **25** (2004) 1873

[27] M. Ishii, J. Hiraishi, T. Yamanaka, Phys. Chem. Minerals. **8** (1982) 64

[28] M. L. Bortz, R. H. French, D. J. Jones, R. V. Kasowski, F. S. Ohuchi, Phys. Scr. **41** (1990) 537

[29] R. A. Evarestov, A. Platonenko, D. Gryaznov, Yu. F. Zhukovskii, E. A. Kotomin, Phys. Chem. Chem. Phys. **19** (2017) 25245.

[30] R. F. W. Bader, Atoms in Molecules - A Quantum Theory, vol. 22 of International Series of Monographs in Chemistry. Oxford, UK: Oxford University Press (1990)

[31] C. Gatti, V. R. Saunders, C. Roetti, J. Chem. Phys. **101** (1994) 10686

[32] E. Wiberg, N. Wiberg, A. F. Holleman, Inorganic Chemistry, Acad. Press, San Diego, 1st English Edn, 2001, p. 1884.

[33] E. Rühl, A. P. Hitchcock, Chem. Phys. **154** (1991) 323

[34] S. J. Zinkle, Mater. Res. Soc. Symp. Proc. **439** (1997) 667

[35] B. P. Uberuaga, D. Bacorisen, R. Smith, J. A. Ball, R. W. Grimes, A. F. Voter, and K. E. Sickafus, Phys. Rev. B **75** (2007) 104116

Table 1 Neutral defect formation energies, bond length (d_{O-O}) and their effective charges

Supercell	Formation energies, eV		d_{O-O}, Å	Effective charges of O_i and O_{reg} (O_i / O_{reg}), *e*	
	F-center	O_i		Mulliken	Hirshfield-I
56 atoms	7.88	2.31	1.42	-0.61/-0.65	-0.83/-0.84
112 atoms	7.92	2.51	1.42	-0.63/-0.64	-0.84/-0.83

Table 2. Configuration of neutral O_i and its surrounding at the top of migration barrier.

Trajectory		I	II	III
Energy barrier, eV		1.0	1.1	2.4
O_i charge, *e*	Mulliken	-0.57	-0.56	-0.55
	Hirshfield-I	-0.71	-0.71	-0.56
NN distance, Å		O_{reg0} 1.66 Å, Al 1.78 Å, O_{reg1} 1.79 Å, Mg 2.07 Å	O_{reg0} 1.72 Å, O_{reg2} 1.77 Å, Al 1.77 Å, Mg 2.08 Å	O_{reg0} 1.63 Å, O_{reg3} 1.77 Å, Mg 1.86 Å, Al 2.33
Bond population of O_i with NN		-0.11, 0.30, -0.28, 0.04	-0.10, -0.24, 0.31, 0.04	-0.09, -0.28, 0.06, 0.04

Table 3. Configuration of c O_i and its surrounding at the top of migration barrier.

Trajectory		I	II
Energy barrier, eV		0.80	0.88
O_i charge, *e*	Mulliken	-0.97	-0.98
	Hirshfield-I	-1.21	-1.26
NN distance, Å		Al 1.76 Å, Mg 1.91 Å, O_{reg1} 1.99 Å O_{reg0} 2.21 Å	Al 1.84 Å, Al 1.87 Å, O_{reg0} 1.99 Å, O_{reg2} 2.03 Å
Bond population of O_i with NN		0.34, 0.06, -0.12, -0.06	0.21, 0.28, -0.18, -0.29

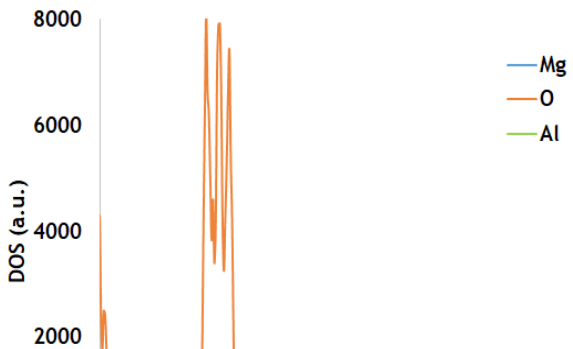

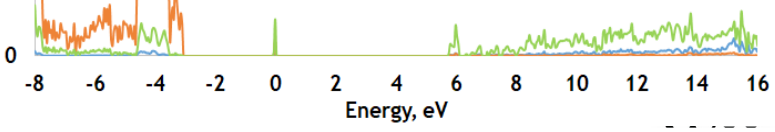

Figure 1. Partial density of states of spinel supercell containing F-center. Zero energy corresponds to the highest occupied energy level.

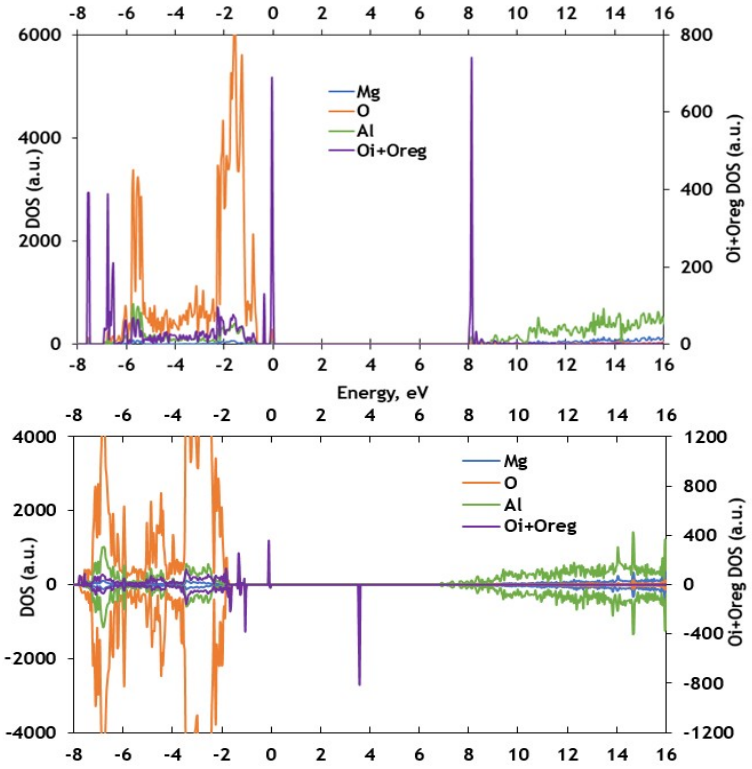

Figure 2. Partial DOS of a neutral (top) and charged (bottom) oxygen interstitials in spinel. The magnitude of DOS of O-O pair is on right y-axis. Zero energy corresponds to the highest occupied energy level. For charged oxygen interstitials positive and negative values correspond to spin-up and spin-down states respectively.

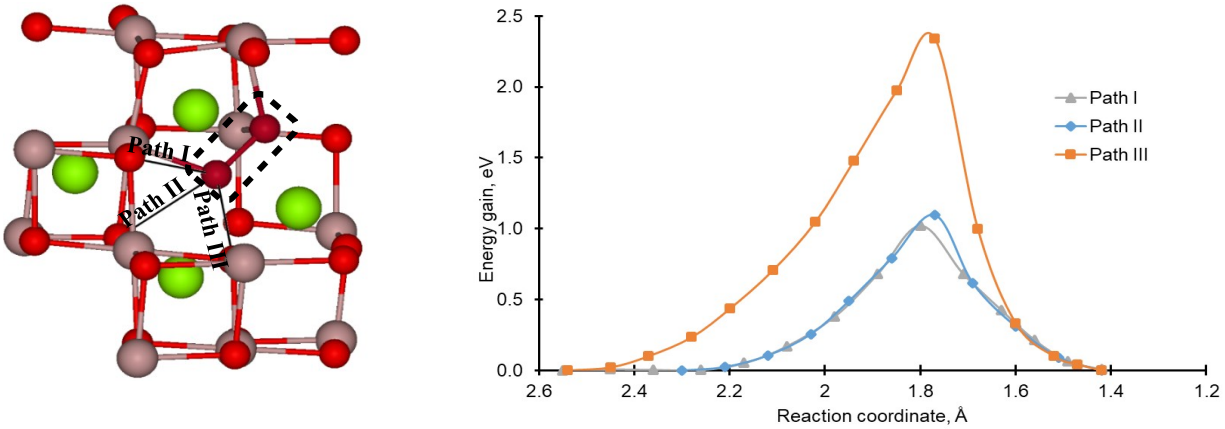

Fig. 3. Left: fragment of 113 atom supercell with three migration paths of neutral Oi in spinel crystal. Green balls correspond to Mg atoms, grey-brown – Al atoms, and red – O atoms. The dumbbell (O-O pair) is shown in dark red and highlighted with dotted rectangle. Right: the energy curves for three migration paths of neutral Oi with estimated energy barriers. The reaction coordinate is the distance between the end atom of a dumbbell and the Oreg ion to which it moves..

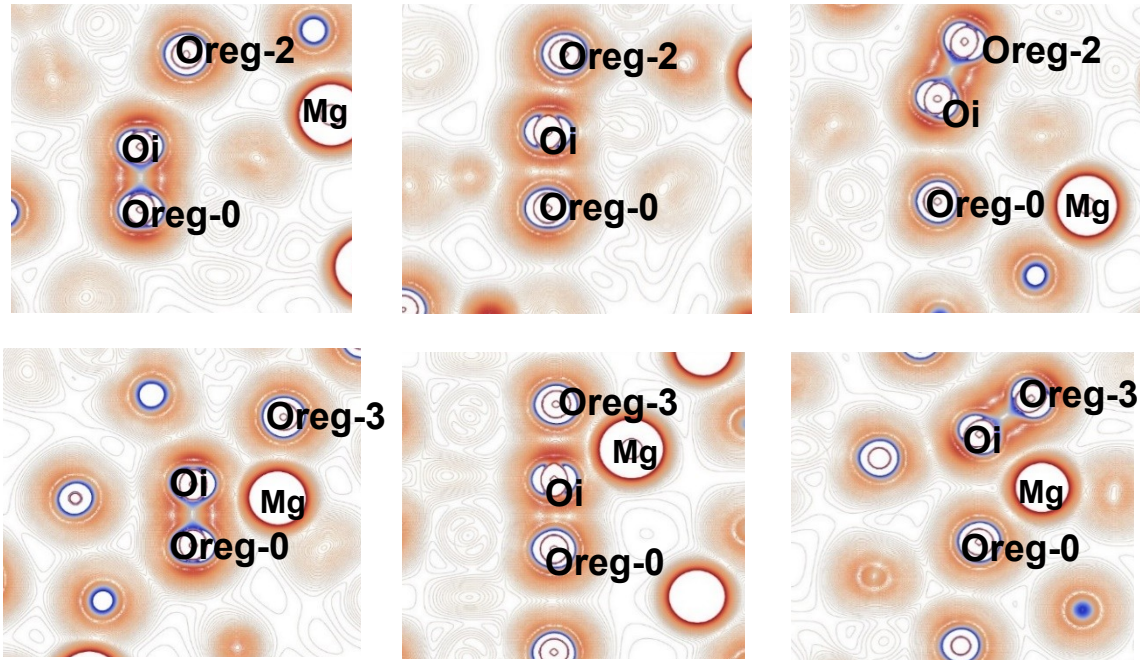

Figure 4. 2D plot of Laplacian of electron density ($\nabla 2\rho$) of defective spinel. Neutral interstitial configurations for paths II (top) and III (bottom) are shown in the dumbbell (left), in the top of energy barrier (center) and the final point (right). All mapped planes are built through Oreg0 – Oi – Oreg2/3 atoms. The formation of bond is seen due to high density blue contours (negative sign of $\nabla 2\rho$) between Oi and regular oxygen atom Oreg0. Migration path lies in the direction of Oreg-2/3.

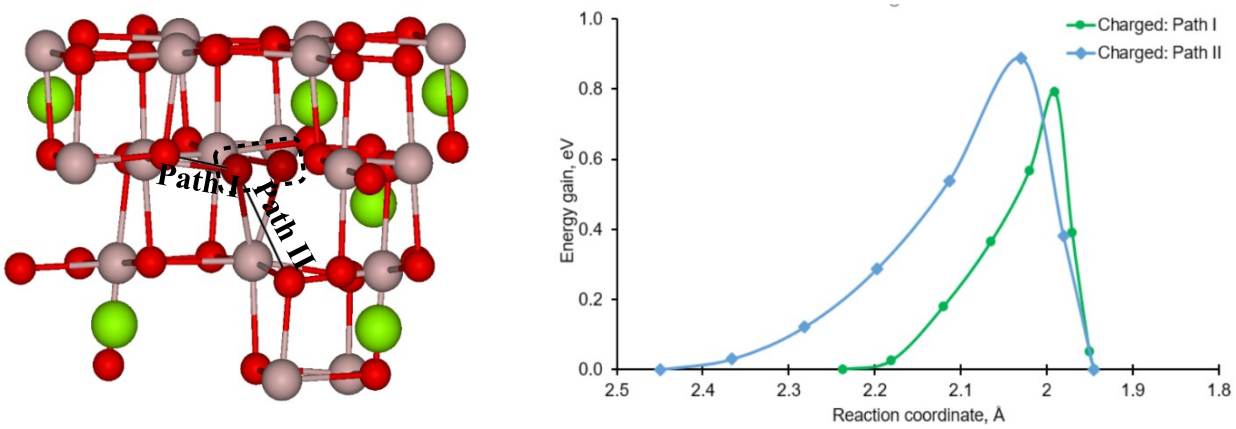

Figure 5. Left: fragment of 113 atom supercell with two migration paths of charged Oi in spinel crystal. OO pair atoms shown in dark red and highlighted with dotted rectangle. Right: Energy curves for migration paths of charged Oi with estimated energy barriers.

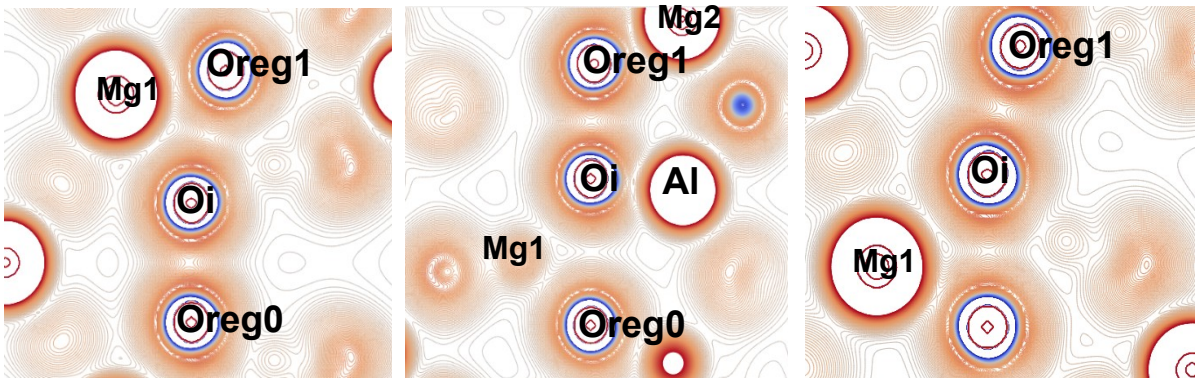

Figure 6. 2D plot of Laplacian of electron density ($\nabla 2\rho$) of defective spinel. Charged interstitial configurations of path I in the starting point (left), in the top of energy barrier (center) and the final point (right) are shown. All mapped planes are built through Oreg0 – Oi – Oreg1 points. Red, blue and grey contours have the same meaning as in Figure 4.